Electronic Structure of the Quinone Radical Anion A(1)(center dot-) of Photosystem I Investigated by Advanced Pulse EPR and ENDOR Techniques

ARTICLE *in* THE JOURNAL OF PHYSICAL CHEMISTRY B · AUGUST 2009

Impact Factor: 3.3 · DOI: 10.1021/jp901890z · Source: PubMed

Electronic Structure of the Quinone Radical Anion $A_1^{\bullet-}$ of Photosystem I Investigated by Advanced Pulse EPR and ENDOR Techniques

Jens Niklas,[†] Boris Epel,[†] Mikhail L. Antonkine,[†,‡] Sebastian Sinnecker,[†] Maria-Eirini Pandelia,[†] and Wolfgang Lubitz*[,†]

Max-Planck-Institut für Bioanorganische Chemie, Stiftstrasse 34-36, 45470 Mülheim/Ruhr, Germany, and Institut für Experimentalphysik, Freie Universität Berlin, Arnimallee 14, 14195 Berlin, Germany

Received: March 1, 2009; Revised Manuscript Received: June 3, 2009

Vitamin K_1 (VK_1) is an important cofactor of the electron-transfer chain in photosystem I (PS I), referred to as A_1. The special properties of this quinone result from its unique interaction(s) with the protein surrounding. In particular, a single H-bond to neutral A_1 was identified previously in the X-ray crystal structure of PS I. During light-induced electron transfer in PS I, A_1 is transiently reduced to the radical anion $A_1^{\bullet-}$. In this work, we characterized the electron spin density distribution of $A_1^{\bullet-}$ with the aim of understanding the influence of the protein surrounding on it. We studied the light-induced spin-polarized radical pair $P_{700}^{\bullet+}A_1^{\bullet-}$ and the photoaccumulated radical anion $A_1^{\bullet-}$, using advanced pulse EPR, ENDOR, and TRIPLE techniques at Q-band (34 GHz). Exchange with fully deuterated quinone in the A_1 binding site allowed differentiation between proton hyperfine couplings from the quinone and from the protein surrounding. In addition, DFT calculations on a model of the A_1 site were performed and provided proton hyperfine couplings that were in close agreement with the ones determined experimentally. This combined approach allowed the assignment of proton hyperfine coupling tensors to molecular positions, thereby yielding a picture of the spin density distribution in $A_1^{\bullet-}$. Comparison with $VK_1^{\bullet-}$ in organic solvents (Epel et al. *J. Phys. Chem. B* **2006**, *110*, 11549.) leads to the conclusion that the single H-bond present in both the radical pair $P_{700}^{\bullet+}A_1^{\bullet-}$ and the photoaccumulated radical anion $A_1^{\bullet-}$ is, indeed, the crucial factor that governs the electronic structure of $A_1^{\bullet-}$.

Introduction

Photosystem I (PS I) is an indispensible part of oxygenic photosynthesis in plants, algae, and cyanobacteria.[1−3] PS I is an integral membrane protein that consists of several subunits and carries a large number of cofactors, including chlorophylls (Chls), carotenoids, FeS clusters, and quinones.[4,5] The two central PS I subunits PsaA and PsaB are arranged in a nearly symmetrical structure, with a pseudo-C_2 axis that runs through the electron donor P_{700} (a dimer of Chls) to F_X, a [4Fe−4S] cluster (Figure 1a). PsaA and PsaB provide the ligands for the majority of the electron-transfer cofactors in PS I. The two branches of the electron-transfer cofactors (termed the A and B branches) are located on both sides of the pseudo-C_2 axis.

P_{700} is followed by two additional Chl *a* molecules on each branch. Light-induced charge separation is initiated within these six excitonically coupled Chl molecules. The nature and kinetics of the primary steps in charge separation are a controversial topic of discussion.[6] Recently, it was proposed that $P_{700}^{\bullet+}$ is generated only after oxidation of the accessory Chl molecules (A_A and A_B; see Figure 1a).[7−9] The first stable intermediate, $P_{700}^{\bullet+}A_0^{\bullet-}$, is generated within a few picoseconds after light excitation. The next electron acceptor A_1 (VK_1) is reached in ∼30 ps.[10] Then, the electron is transferred to F_X, which is a [4Fe−4S] cluster bound to PsaA and PsaB. The PsaC-bound [4Fe−4S] clusters F_A and F_B follow in the electron-transfer chain.[11−13] In less than 1 ms, the electron reaches the terminal electron acceptor F_B, located on the stromal side.

After the initial electron-transfer steps, the quinone becomes singly reduced, and the spin-polarized radical pair (RP) $P_{700}^{\bullet+}A_1^{\bullet-}$ is formed.[14−16] It has been a matter of controversy whether one or two branches are active under different experimental conditions, that is, whether the quinone in the A branch, the quinone in the B branch, or both quinones participate in electron transfer.[17−26] Most likely, the quinones in both branches take part in electron transport at physiological temperatures. It has been shown that, at cryogenic temperatures, reversible charge separation takes place in the A branch, as can be observed by time-resolved EPR spectroscopy.[14,18,19,27−29]

The structure of the A_1 site in the A branch of PS I in the 2.5 Å X-ray crystal structure is shown in Figure 1b (PDB entry 1JB0).[4] The A_1 site in the B branch is identical within the resolution of the X-ray structure. Figure 1c shows the chemical structures of VK_1 and VK_3. In the A_1 site, the backbone amide proton of a leucine residue is within a H-bonding distance from the C−O group at position 4 of VK_1, whereas in the symmetric position 1, no potential H-bonding donor is present. A tryptophan residue is in a π-stacked arrangement to the quinone, with a plane-to-plane distance of 3.0−3.5 Å. Note that the X-ray structure has been solved for PS I with A_1 in the neutral state. X-ray crystallography does not provide information about the structure and dynamics of PS I with reduced A_1. EPR spectroscopy showed previously that the spatial arrangement of the quinone in the charge-separated state $P_{700}^{\bullet+}A_1^{\bullet-}$ is similar to that of the neutral quinone.[14,19,29]

The protein-bound VK_1 has a very low redox potential ($E_m \approx -800$ mV).[13,30,31] One of the major goals of the research on $A_1^{\bullet-}$ is to understand how the protein modulates the quinone properties inside PS I, that is, how the low reduction potential

* Corresponding author. E-mail: lubitz@mpi-muelheim.mpg.de.
[†] Max-Planck-Institut für Bioanorganische Chemie.
[‡] Freie Universität Berlin.

10.1021/jp901890z CCC: $40.75
Published on Web 07/09/2009

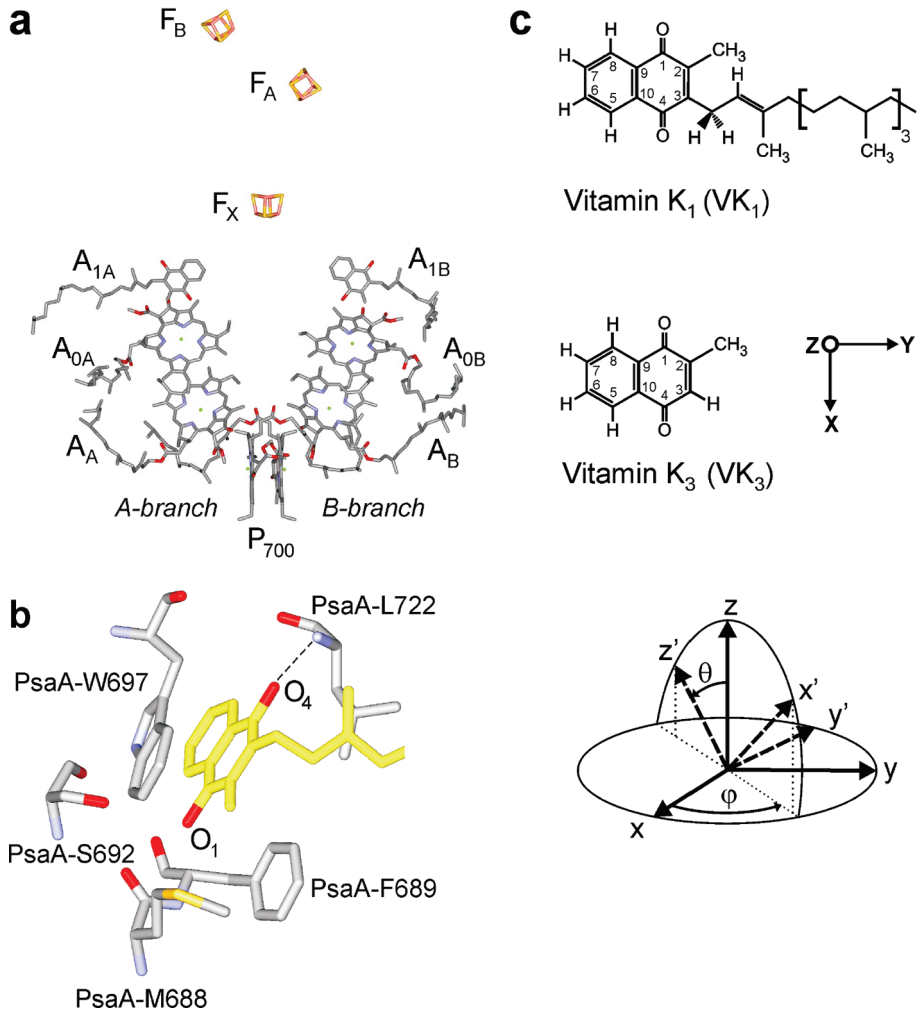

Figure 1. (a) Arrangement of the cofactors in the electron-transfer chain of PS I from *T. elongatus* taken from the 2.5 Å X-ray crystal structure (PDB entry 1JB0).[4] The two branches are denoted as the A branch and the B branch. The spectroscopic names are indicated for each cofactor, and A_A and A_B denote the accessory Chl molecules. The use of A or B in the subscript of the names indicates the respective branch. (b) Structure of the A_1 binding site in the A branch of PS I taken from the 2.5 Å crystal structure (PDB entry 1JB0).[4] The corresponding B-branch binding site is almost identical. The quinone vitamin K_1 (VK_1; phytyl chain truncated) is depicted in yellow with oxygen atoms colored red. The color coding within amino acids is as follows: carbon, gray; oxygen, red; nitrogen, blue; sulfur, yellow. The backbone amide proton of Leu A722 (PsaA-L722) is within a H-bonding distance to O_4 of VK_1 (indicated by a dashed line; $d_{N-O} = 2.7$ Å), whereas in the symmetric position of the quinone (position O_1), no H-bonding donor is present. Trp A697 (PsaA-W697) is π-stacked to the quinone with a plane-to-plane distance of 3.0−3.5 Å. Three other important residues are also shown. (c) Chemical structures of the quinones vitamin K_1 (VK_1) and vitamin K_3 (VK_3) together with numbering schemes. The α-protons are bound directly to the aromatic rings, and the β-protons are found within the methyl group and the first CH_2 group of the phytyl chain of the quinone molecules. The principal axes of the **g** tensor are expected to be collinear with the shown molecular axes system. The *x* and *y* principal axes lie in the quinone plane, with the *x* axis parallel to the C−O bond, and the *z* axis is perpendicular to the quinone plane.[106,107]

of the quinone is achieved. Various quinones can be incorporated into the A_1 binding site, and similarly low redox potentials are achieved with these quinones.[19,32−36] Thus, the low redox potential of the quinone is conferred by the A_1 binding site.

The electronic structure of $VK_1^{\bullet-}$ in the A_1 binding site is different from that of $VK_1^{\bullet-}$ in organic solvents.[37−39] The electron spin density distribution represents a sensitive probe of the electronic structure. So far, the spin density distribution in $A_1^{\bullet-}$ is not fully known. The influence of protein−cofactor interactions on the electronic structure of the quinone, and thus the spin density distribution, is a controversial topic in the literature, for example, with respect to the impact of the H-bond and the π-stacked tryptophan.[14,40] Of special interest is the interaction of the protein surrounding with the quinone through a single hydrogen bond as compared to the bacterial photosynthetic reaction center, where the quinone in the Q_A site is bound to the protein through two H-bonds.[41−44]

The electron spin density distribution can be directly probed by the ^{1}H hf interaction.[41,45−48] The ^{1}H hfc constants, however, are often too small to be resolved in the EPR spectrum, necessitating the use of advanced EPR techniques such as ^{1}H ENDOR spectroscopy to increase the spectral resolution. The radical anion $A_1^{\bullet-}$ was investigated by ^{1}H ENDOR spectroscopy previously (see, e.g., refs 28, 36, 37, 39, and 49−51). However, only the hfc tensor of the freely rotating methyl group protons has been determined and definitively assigned so far.[37] Other spectral features have been assigned in different ways by several groups (see, e.g., refs 39, 49, and 50). A problem of previous ENDOR studies on $A_1^{\bullet-}$ is the poor spectral resolution at X-band, where nearly all of these studies were performed. The situation is different at Q-band, where a better spectral resolution is achieved.

A further drawback of many of the previous ENDOR studies was that only photoaccumulated $A_1^{\bullet-}$ was studied.[37,49,50,52−54] This presents a two-fold problem: (i) $A_1^{\bullet-}$ in the functionally relevant RP $P_{700}^{\bullet+}A_1^{\bullet-}$ was not studied, and (ii) PS I samples with photoaccumulated $A_1^{\bullet-}$ often contain a significant amount of the chlorophyll radical anion $A_0^{\bullet-}$, which has overlapping

EPR and ^{1}H ENDOR spectra with $A_1^{\bullet-}$. Experiments on the RP offer the advantage of looking directly at the functionally relevant RP $P_{700}^{\bullet+}A_1^{\bullet-}$ not contaminated by stationary signals. Note, however, that the analysis of the RP ENDOR spectra is rather complicated; thus, only a partial analysis of the spectra has been published to date.[51]

The problem of assigning ^{1}H ENDOR signals to particular protons can be addressed in different ways. One strategy is to modify the protein environment by introducing single-point mutations (see, e.g., refs 28, 52, and 53). Unfortunately, this method often alters the structure of the protein and the cofactors. Another approach is to use isotopic labeling, which does not perturb the system and which is used here. A straightforward way to disentangle proton hfc constants from the quinone and its protein environment is deuteration of either the quinone or its surrounding.

Effective exchange of the quinone in the A_1 site is an essential prerequisite for studies which use labeled quinones. Here, we use PS I isolated from the *Synechocystis menB*26 mutant.[55] In *menB* strains, the pathway for biosynthesis of VK_1 is interrupted by interposon mutagenesis of the *menB* gene in *Synechocystis* sp. PCC 6803.[56,57] This results in PS I complexes where PQ_9 instead of VK_1 (Figure S1, Supporting Information) occupies the A_1 binding site.[36,56] The binding of PQ_9 is much weaker than that of the native VK_1, so PQ_9 can easily be exchanged with other quinones with higher affinity to the A_1 binding site, such as VK_1 or VK_3.[49,55] The latter is a close analog of VK_1 that is lacking the phytyl chain at position 3 (Figure 1c). In the present study, VK_1 and VK_3 (VK_3-h_8 and VK_3-d_8) were used for the substitution of PQ_9 in the A_1 binding site of PS I isolated from *Synechocystis menB*26. Previous EPR measurements have shown that the substituted VK_3 is positioned and oriented identically to the native VK_1 in the A_1 binding site.[49,58]

Our previous study of $VK_1^{\bullet-}$ and related quinone radical anions in organic solvents by pulse Q-band EPR, ENDOR, and TRIPLE spectroscopy and DFT calculations yielded a comprehensive assignment of ^{1}H hfc tensors to molecular positions.[59] Building on these results, the same combination of advanced methods was applied here to address the corresponding problem of the radical anion $VK_1^{\bullet-}$ in the A_1 binding site of PS I. Measurements were performed both on $A_1^{\bullet-}$ in the short-lived spin-polarized RP $P_{700}^{\bullet+}A_1^{\bullet-}$ and on the photoaccumulated radical anion $A_1^{\bullet-}$. Additionally, novel pulse ENDOR techniques (variable-mixing-time ENDOR[60−62] and one- and two-dimensional TRIPLE[63−65]) were used here to obtain the signs of the hfc constants as well as the orientation of the hfc tensors. To investigate the influence of the protein surrounding on the hfc tensors, the proton hfc tensors obtained for $VK_1^{\bullet-}$ and $VK_3^{\bullet-}$ in the A_1 binding site of PS I are compared to the proton hfc tensors obtained for $VK_1^{\bullet-}$ and $VK_3^{\bullet-}$ in organic solvents. Our results explain the observed changes in the distribution of electron spin density by interaction of the quinone with the protein surrounding.

Materials and Methods

Biochemical Preparations. Growth of the thermophilic cyanobacterium *Thermosynechococcus elongatus* (*T. elongatus*) and isolation of PS I was done as described previously.[66] The trimeric PS I complexes isolated from this organism were obtained from P. Fromme (Arizona State University, Tempe, AZ) and J. Frank and J. Kern (TU Berlin, Berlin, Germany).

Growth of the *Synechocystis menB*26 strain was performed as described previously.[55] The procedure used for the isolation of trimeric PS I complexes is a modification of the one used previously.[67]

For the quinone exchange in the A_1 binding site, PS I from *Synechocystis menB*26 was used. The procedure was based on previous studies.[49,58] A detailed description of the quinone exchange procedure is provided in the Supporting Information.

PS I samples from *T. elongatus* and *Synechocystis menB*26 contained between 0.1 and 0.2 mM PS I. The samples for RP measurements were reduced by adding sodium ascorbate (final concentration of 5 mM), incubated in the dark for 5 min at 4 °C, and then quickly frozen in liquid nitrogen in the dark. The photoaccumulated quinone radical anion $A_1^{\bullet-}$ was generated using procedures similar to those previously described.[68] The FeS clusters were prereduced by sodium dithionite[12,69] and then the sample was illuminated to generate the quinone radical anion $A_1^{\bullet-}$. A detailed description is provided in the Supporting Information.

EPR and ENDOR Measurements. All EPR and ENDOR experiments were carried out on a Bruker ELEXSYS E580 Q-band spectrometer with a Super Q-FT microwave bridge equipped with a home-built ENDOR resonator,[70,71] similar to the one described in ref 72. The resonator used for measurements on the light-induced RP $P_{700}^{\bullet+}A_1^{\bullet-}$ contained 12 horizontal slits of 0.3-mm width to allow in situ light excitation of the sample (>65% light transmission). All pulse EPR and ENDOR spectra of the light-induced RP $P_{700}^{\bullet+}A_1^{\bullet-}$ were corrected for the dark background recorded 10 ms after the Laser flash. Variable-Mixing-Time (VMT) ENDOR experiments based on the Davies ENDOR sequence[73] were performed to determine the absolute signs of the ^{1}H hfc constants of $A_1^{\bullet-}$ in the RP as described previously.[60] To determine the (relative) signs of the hfc constants in the photoaccumulated radical anion $A_1^{\bullet-}$, one-dimensional pulsed electron−nuclear−nuclear TRIPLE resonance was used.[63] Two-dimensional pulsed electron−nuclear−nuclear TRIPLE resonance experiments were employed to obtain the relative signs of hfc constants and the orientations of hfc tensors.[64,65] All TRIPLE experiments were based on the Davies ENDOR sequence.[73] Further details are provided in the Supporting Information.

Spectral Simulations. All data-processing routines and simulations were performed in the MATLAB environment,[74] using the EasySpin software package (version 2.7.1).[75] For ENDOR and TRIPLE simulations the EasySpin package together with home-written routines was used.[59] Simulations of the EPR spectra of the spin-polarized RP $P_{700}^{\bullet+}A_1^{\bullet-}$ were performed with the program of Salikhov and co-workers.[76−78] The three protons of the methyl group (the only strongly coupled protons in $A_1^{\bullet-}$) were included in the simulation of all EPR spectra. Simulations of the ENDOR spectra of the spin-polarized RP $P_{700}^{\bullet+}A_1^{\bullet-}$ were done using procedures similar to those used for stationary radicals.[59] The principal values of the ^{1}H hfc tensors and the orientation of the principal axes with respect to the **g**-tensor principal axes are summarized in Table 1 for VK_1 and in Table 2 for VK_3.

DFT Calculations on $VK_1^{\bullet-}$ and $VK_3^{\bullet-}$ in the A_1 Binding Site. For the DFT calculations, the smallest feasible model systems were chosen. They contain either VK_1 (with a truncated phytyl chain; see Figure S1, Supporting Information) or VK_3 and the backbone of the two amino acids alanine (PsaA-A721) and leucine (PsaA-L722). The amide nitrogen of the leucine is involved in a hydrogen bond with the oxygen at position 4 of the quinone (Figure 1b). The coordinates for the geometry optimizations were taken from the X-ray crystal structure of

TABLE 1: ^{1}H hfc Constants of $VK_1^{\bullet-}$ in the A_1 Binding Site of PS I from *T. elongatus* Determined Experimentally and from DFT Calculations (MHz)

	position 2 (CH_3)[a]		position 3 (CH_2)		position 5 (α)		position 6 (α)		position 7 (α)		position 8 (α)		H-bond	
	expt	DFT	expt	DFT	expt	DFT	expt	DFT	expt	DFT	expt	DFT	expt	DFT
A_x	+8.8	+9.62		−0.85	−1.9	−1.84	−2.1	−1.74	−5.0	−5.19	−0.8	−0.65	+7.4	+7.27
	(+9.1)[b]			+2.53	(−1.9)		(−2.0)		(−5.2)		(−0.8)		(+7.4)	
A_y	+12.4	+13.05		+3.72	(−0.3)	−0.07	(+0.5)	+0.66	(−0.7)	−0.68	(+3.5)	+3.56	(−3.5)	−4.31
	(+12.7)			+5.16										
A_z	+8.3	+8.86	(+1.6)	−2.01	(−3.6)	−3.56	(−1.9)	−1.59	−3.50	−3.72	(−1.3)	−1.55	(−3.5)	−3.78
	(+8.6)			+1.68					(−3.40)					
a_{iso}	+9.8	+10.51		+0.29	(−1.9)	−1.82	(−1.1)	−0.89	(−3.1)	−3.19	(+0.5)	+0.46	(+0.1)	−0.28
	(+10.1)			+3.12										
φ[c]	+30	+14		−22	+12	+12	+10	+10	−12	−22	−5	−5	−20	−30
				−14										
θ[c]	0	+1		+4[d]	0	−5	0	−6	0	−2	0	+1	+30	+12
				−10[d]										

[a] Numbering of molecular positions is according to Figure 1c. [b] Values in parentheses refer to the photoaccumulated radical anion $A_1^{\bullet-}$. [c] Angles (φ, θ) of the hfc tensor principal axes with respect to the principal axes of the **g** tensor are given in degrees; see Figure 1c for the definition. Angles are assumed to be identical in the RP and the photoaccumulated radical anion. The error in the determination of the hfc constants is typically in the order of 100 kHz, but can be larger in some cases of broad or overlapping lines (e.g., the H-bond proton). The precision of the determination of the angles (φ, θ) is <10° for the methyl group protons, the strongly coupled α-proton of the benzoic ring, and the H-bond proton. This precision is especially due to the sensitivity of the 2D TRIPLE spectrum to the orientation of the hfc tensor principal axes. For the more weakly coupled protons, the errors in the angles are larger. [d] These are the only protons for which the A_y component is also significantly out-of-plane (>4°).

TABLE 2: ^{1}H hfc Constants of $VK_3^{\bullet-}$ in the A_1 Binding Site of PS I from *Synechocystis menB*26 Mutant Determined Experimentally and from DFT Calculations (MHz)

	position 2 (CH_3)[a]		position 3 (α)		position 5 (α)		position 6 (α)		position 7 (α)		position 8 (α)		H-bond	
	expt	DFT	expt	DFT	expt	DFT	expt	DFT	expt	DFT	expt	DFT	expt	DFT
A_x	+8.7	+8.82	−7.6	−7.20	−1.8	−1.55	−2.5	−2.28	−4.6	−4.67	−0.8	−0.85	+7.4	+7.38
A_y	+12.3	+12.40		+0.38		+0.41		+0.42		−0.49		+3.18		−4.42
A_z	+8.2	+8.02	−6.7	−7.16		−3.16		−1.92	−3.1	−3.40		−1.83		−3.85
a_{iso}	+9.7	+9.77		−4.66		−1.44		−1.26		−2.86		+0.17		−0.30
φ[b]	+25	+10	−15	−17	+4	+7	+12	+10	−20	−25	−14	−8	−20	−32
θ[b]	0	−2	0	0	0	−4	0	−3	0	−2	0	−1	+30	+12

[a] Numbering of molecular positions is according to Figure 1c. [b] Angles (φ, θ) of the hfc tensor principal axes with respect to the principal axes of the **g** tensor are given in degrees; see Figure 1c for definition. The angles were − aside from the H-bond proton – taken from measurements on $VK_3^{\bullet-}$ in 2-propanol.[59] The error in the determination of the hfc constants is typically in the order of 100 kHz, but can be larger in some cases of broad or overlapping lines (e.g., the H-bond proton or the α-proton at position 3).

cyanobacterial PS I (PDB entry 1JB0).[4] Computational details are provided in the Supporting Information.

Results

Integrity of the A_1 Binding Site. This work takes advantage of PS I samples with different quinones in the A_1 binding site. A prerequisite for all spectroscopic studies described here is the integrity of this site after incorporation of different quinones into PS I. This was addressed by transient EPR and pulse ^{1}H ENDOR spectroscopy, which showed that (i) PQ_9 could be quantitatively replaced in vitro by VK_1 or VK_3 in the A_1 binding site of PS I isolated from *Synechocystis menB*26 mutant, (ii) the A_1 site structure and functional activity is preserved after the quinone replacement procedure, and (iii) the A_1 binding sites in the thermophilic *T. elongatus* and the mesophilic *Synechocystis* strains are similar.

In general, the RP EPR spectra can be described as a superposition of emissive and absorptive spectra of $A_1^{\bullet-}$ and $P_{700}^{\bullet+}$.[38,79−81] The signal of $P_{700}^{\bullet+}$ dominates the central and high-field regions of the spectra, whereas the low-field region of the EPR spectra contains a significant contribution of the $A_1^{\bullet-}$ signal, which exhibits a larger **g** anisotropy. The evaluation of the degree of quinone exchange was done as described previously by inspection of the low-field wing of the transient EPR spectra of the RP.[49] The exchange was estimated to be better than 95%. The RP EPR spectra are very sensitive to the orientation of the two cofactors with respect to each other. The good agreement with the simulations, which used the same interaction tensor and the same orientation of the two **g** tensors as for wild-type PS I, assured that the substituted quinones were bound in the same position and orientation [see Table S1 (Supporting Information) for the principal values of the **g** tensors].

The similarity of the A_1 binding sites in PS I isolated from *T. elongatus* (with native VK_1) and *Synechocystis menB*26 substituted with VK_1 is evident from comparison of the RP ENDOR spectra (Figure S2, Supporting Information). Furthermore, this is an additional strong indication that the quinone substitution procedure does not alter the A_1 binding site. The differences in the ENDOR spectra of $A_1^{\bullet-}$ arising upon quinone substitution with VK_3 in PS I from *Synechocystis menB*26 result solely from differences between the radicals $VK_1^{\bullet-}$ and $VK_3^{\bullet-}$.

For the analysis of the ^{1}H ENDOR spectra of photoaccumulated $A_1^{\bullet-}$, it is important to ensure the absence of contaminating radicals. In particular, the chlorophyll anion radical $A_0^{\bullet-}$ is a common contaminant in this type of samples (e.g., refs 37, 49, and 82). The prominent broad lines belonging to $A_0^{\bullet-}$ (hfc constants > 10 MHz) are very weak in the ENDOR spectra recorded around the g_z position of $A_1^{\bullet-}$ in our *T. elongatus* samples (see discussion and comparison of ENDOR spectra in

Figure S3, Supporting Information). Under identical photoaccumulation conditions, PS I isolated from *Synechocystis menB*26 accumulated a significant amount of $A_0^{\bullet-}$. Therefore, PS I isolated from *Synechocystis menB*26 was investigated only by RP ENDOR spectroscopy.

Pulse ENDOR and TRIPLE Measurements. To determine the orientation of the hfc tensor principal axes with respect to the **g**-tensor axes and to increase the spectral resolution, molecules that have different orientations with respect to the magnetic field have to be excited.[83−85] For a complete orientation selection, all principal components of the **g** tensor must be resolved in the EPR spectrum. In the Q-band EPR spectrum of photoaccumulated $A_1^{\bullet-}$, only the g_z component is well separated from the other **g**-tensor components, whereas the g_x and g_y components are partially separated. This means that only in the ENDOR spectra recorded close to the g_z spectral position (high-field edge) can single crystal-like ENDOR spectra be obtained. ENDOR spectra recorded at the low-field edge (close to the g_x orientation) will be close to single-crystal-like, but will still contain signals from molecules with their x axis (parallel to the C−O bonds) slightly tilted with respect to the static magnetic field. At intermediate field positions, the ENDOR spectra show powder patterns.

The RP EPR spectra can be described in a simplified way as a superposition of emissive and absorptive spectra of both $A_1^{\bullet-}$ and $P_{700}^{\bullet+}$. This results in overlap of emissive and absorptive ENDOR signals from $A_1^{\bullet-}$ and $P_{700}^{\bullet+}$ (essentially an overlap of four ENDOR spectra). Furthermore, because of the coupling of the two electron spins (mixture of singlet and triplet states), additional ENDOR signals can appear that are not present in the isolated radicals.[51] The polarization of ENDOR lines of one nucleus can be different (e.g., low-frequency ENDOR transition absorptive, high-frequency ENDOR transition emissive) and depend on the sign of the hfc.[51] This results in congested ENDOR spectra that are very difficult to analyze. It was found previously[60] that the ^{1}H ENDOR spectra recorded at the low-field edge of the RP EPR spectrum show only ENDOR signals from $A_1^{\bullet-}$, and both ENDOR lines of a specific nucleus have the same polarization (emissive). At the high-field edge, the situation is more complicated, because the g_z values of $P_{700}^{\bullet+}$ and $A_1^{\bullet-}$ are close to each other. At intermediate field positions, the ENDOR spectra are further congested because of the overlapping powder patterns (data not shown), and only a few hfc constants (e.g., of the spectrally well separated methyl group protons) could be determined.

In the following discussion, only the ENDOR spectra recorded at the low-field edge are compared. (Additional RP ENDOR spectra were recorded at different magnetic field positions; data not shown.) This field position corresponds to the g_x spectral position of $A_1^{\bullet-}$ (subsequently, g values and orientations with respect to the **g** tensor refer to $A_1^{\bullet-}$ and not to $P_{700}^{\bullet+}$).

In Figure 2, the ^{1}H ENDOR spectra of (a) $A_1^{\bullet-}$ in photoaccumulated and (b) RP samples in PS I from *T. elongatus* and of RP samples in PS I from *Synechocystis menB*26 with (c) VK_3-h_8 and (d) VK_3-d_8 in the A_1 binding site are presented, recorded at the low-field edge (see also Figure S2, Supporting Information). In the ENDOR spectra of $A_1^{\bullet-}$ in photoaccumulated (Figure 2a) and RP samples (Figure 2b) of PS I from *T. elongatus*, signals from protons of VK_1 and the protein surrounding (including the H-bond proton) are present. These spectra are nearly identical with respect to number and positions of the ENDOR lines. In the RP ENDOR spectrum of PS I from *Synechocystis menB*26 substituted with VK_3-h_8 (Figure 2c), the

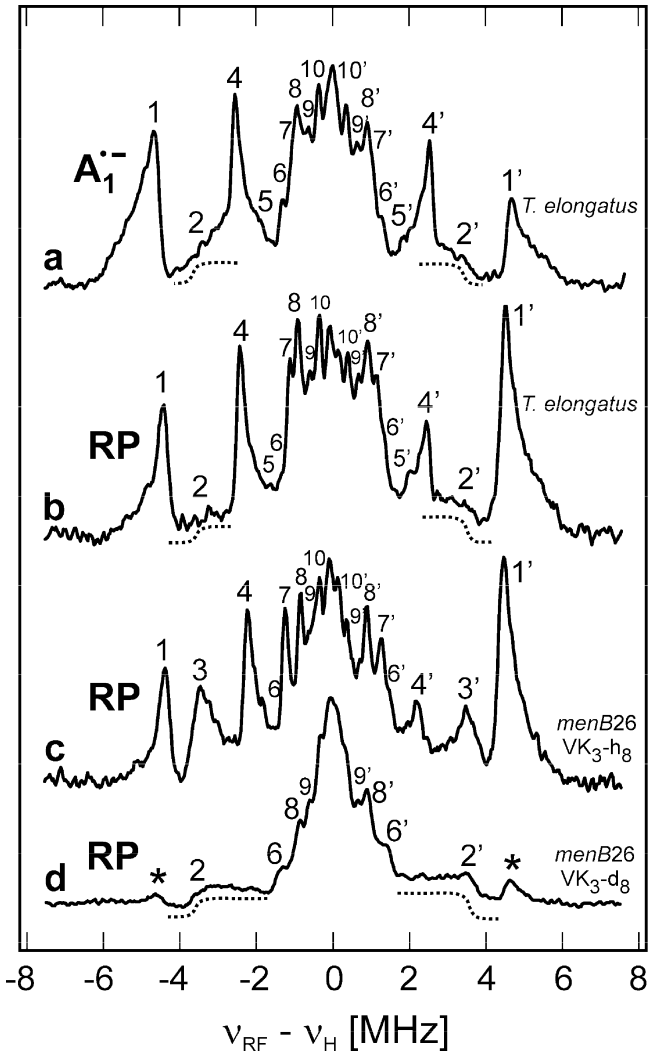

Figure 2. Pulse Q-band ^{1}H Davies ENDOR spectra recorded at the low-field edge of the EPR spectrum of photoaccumulated $A_1^{\bullet-}$ and the RP in PS I from *T. elongatus* and the *Synechocystis menB*26 mutant (T = 80 K). The largest component of the H-bond proton signal ($A_{||}$) is marked by a dotted line for better visualization. The numbering of the ENDOR lines is identical to that in Figures 3 and 4 below; it does not refer to molecular positions. Note that all ENDOR lines of the RP are emissive and are only for comparison with the ENDOR spectrum of the photoaccumulated radical anion $A_1^{\bullet-}$ presented as absorptive ENDOR spectra. (a) Photoaccumulated $A_1^{\bullet-}$ in *T. elongatus* PS I (absorptive ENDOR; see Figure 3a). (b) RP in *T. elongatus* PS I. (c) RP in *Synechocystis menB*26 PS I with VK_3-h_8 in the A_1 binding site. (d) RP in *Synechocystis menB*26 PS I with VK_3-d_8 in the A_1 binding site. The ENDOR signals of the impurity from ∼3% non-deuterated VK_3 are marked with asterisks.

signals of the α-proton at position 3 in the quinone ring can also be observed. Further differences may be due to slightly different hfc tensors of $VK_1^{\bullet-}$ and $VK_3^{\bullet-}$ [59] and the absence of the methylene protons of the phytyl chain in VK_3 (Figure 1c). In the PS I sample from *Synechocystis menB*26 substituted with fully deuterated VK_3-d_8 (Figure 2d), only signals from protons of the protein are expected in the ^{1}H ENDOR spectrum. The respective spectrum exhibits a broad line pair 2/2′, which is hidden in the sample substituted with VK_3-h_8 (Figure 2c). We assign the related hfc to the H-bond proton between leucine PsaA-L722 and the quinone oxygen O_4 (Figure 1b; see also discussion below).

The narrow lines observed in the ^{1}H ENDOR spectra of the samples with protonated VK_1/VK_3 in the A_1 binding site (Figure

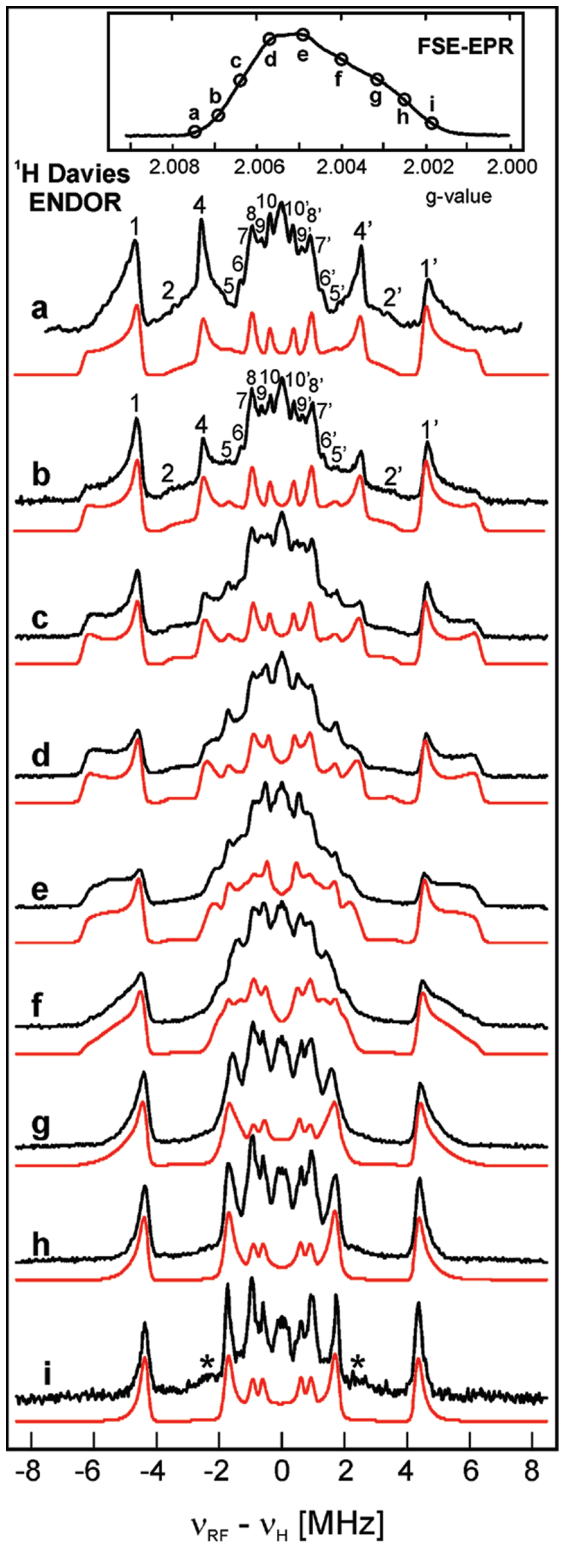

Figure 3. Orientation-selected pulse Q-band ^{1}H Davies ENDOR spectra of the photoaccumulated radical anion $A_1^{\bullet-}$ in *T. elongatus* PS I recorded at different values of the magnetic field (T = 80 K). The inset (top) shows the reference field-swept echo (FSE) detected EPR spectrum. The field positions at which the presented ENDOR spectra were measured are marked with letters. For each field position, the experimental spectrum (black) and the simulation (red) are presented. The numbering of the ENDOR lines is identical to that in Figures 2 and 4. The hfc tensors of the methyl group protons, the H-bond proton, and the four α-protons from the second (benzoic) ring are included in the simulation (see Table 1). The asterisks mark ENDOR lines that are due to the contaminating radical anion $A_0^{\bullet-}$ (see Supporting Information for discussion).

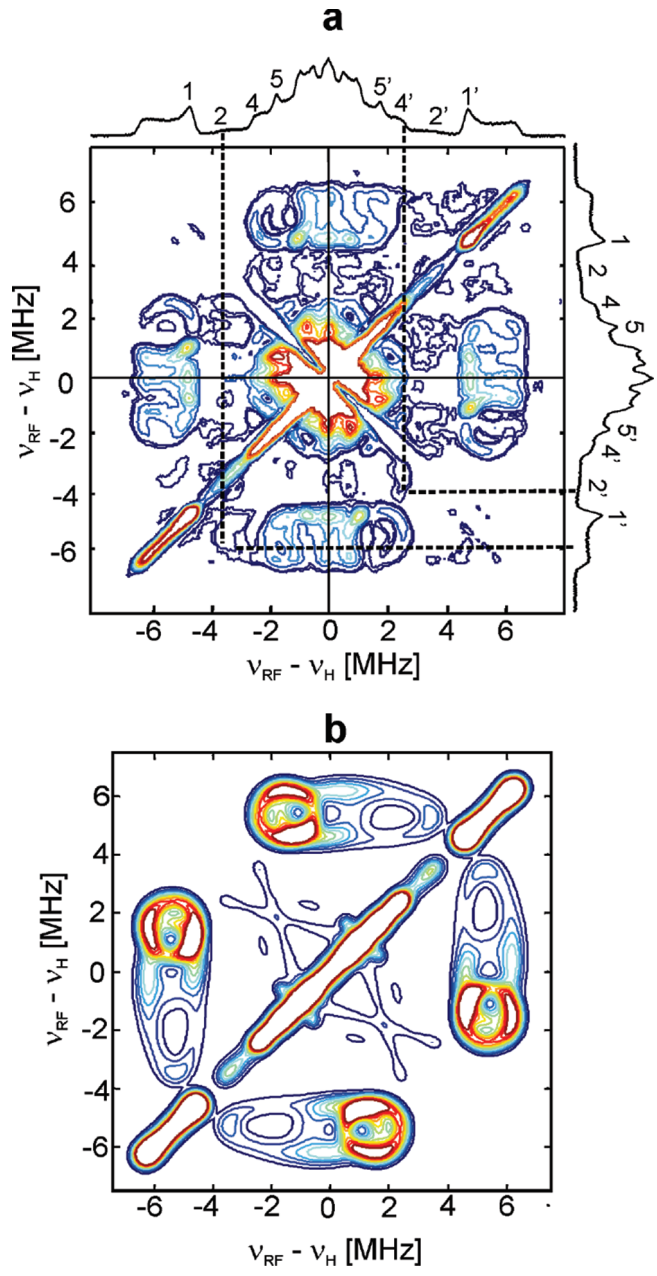

Figure 4. Two-dimensional pulse Q-band difference Davies TRIPLE spectra (^{1}H) of the photoaccumulated radical anion $A_1^{\bullet-}$ in PS I from *T. elongatus*, recorded approximately at the g_y position (T = 80 K). The correlation ridges between the protons with the same sign of the hfc are located in the left quadrant [see, e.g., the correlation between methyl group protons (1′) with the line 2], whereas the correlations between protons with different signs are located in the right quadrant (see, e.g., the correlations between lines 2′ and 4′). On top and at the right edge, the ^{1}H ENDOR spectra recorded at this spectral orientation are given. The numbering of the ENDOR lines is identical to that in Figures 2 and 3. (a) Experiment. (b) Simulation including the three methyl group protons, the H-bond proton, and the proton at position 7 in the benzoic ring.

2a−c) indicate a well-defined binding of the quinone in the protein and the absence of structural heterogeneity. The similarity between the ^{1}H ENDOR spectra of $A_1^{\bullet-}$ in the RP and of photoaccumulated $A_1^{\bullet-}$ of PS I from *T. elongatus* (Figure 2a,b), recorded close to the g_x orientation of $A_1^{\bullet-}$, indicate that the binding of VK_1 is identical, despite the difference in sample preparation. The spectra of samples with protonated VK_1/VK_3 in the A_1 binding site show (Figure 2a−c), for example, the intense line pair 1/1′ due to a large proton hfc of about 9 MHz,

which is assigned to the magnetically equivalent methyl group protons (position 2).[37,39,50,51] This hfc is very similar for VK_3-h_8 in PS I from *Synechocystis menB*26 and native VK_1 in *T. elongatus*. VK_3-d_8 has a degree of deuteration of 97%. Observation of the weak traces of the methyl proton of VK_3-h_8 in PS I from *Synechocystis menB*26, substituted with VK_3-d_8, shows that PQ_9 is quantitatively substituted under our experimental conditions.

The methyl group proton hfc of $A_1^{\bullet-}$ in the RP is decreased by about 300 kHz as compared to that of the photoaccumulated radical (Table 1). A similar difference between RP and photoaccumulated radicals was also observed at X-band.[39,51] The interaction between the two unpaired electrons in the RP as compared to the photoaccumulated radical anion can be excluded as a possible reason for this effect based on a previous study.[51] A potential contributor to this difference is a negative charge on the FeS cluster F_X in the photoaccumulated PS I samples.

In the ENDOR spectra of PS I from *T. elongatus* (Figure 2a,b) and PS I from *Synechocystis menB*26 substituted with VK_3-d_8 (Figure 2d), a broad signal due to a hfc of 7.4 MHz is observed (line pair 2/2′; shoulders are underlined with dotted lines for better visualization). In the ENDOR spectrum of PS I from *Synechocystis menB*26 substituted with VK_3-h_8 (Figure 2c), this line pair is not visible because of overlap with another, more intense line pair (3/3′). Similar signals were also observed by Teutloff et al. for $A_1^{\bullet-}$ in PS I from *T. elongatus*[39] and by Pushkar et al. in photoaccumulated $A_1^{\bullet-}$ in PS I from *Synechocystis menB*26, substituted with VK_3-d_8, and assigned to the $A_{||}$ component of the H-bond proton hfc tensor.[49] A detailed explanation and discussion of the assignment of this hfc is given below.

The intense line pair 3/3′ is visible only in the sample substituted with VK_3-h_8 (Figure 2c). It was shown previously that $VK_3^{\bullet-}$ and $VK_1^{\bullet-}$ exhibit very similar spin densities in organic solvents.[59] Thus, the line pair 3/3′ is assigned to the α-proton at position 3 of the quinone ring that is present in $VK_3^{\bullet-}$ only.

The intense line pair 4/4′ is observed in the ENDOR spectra of the RP and photoaccumulated samples of PS I from *T. elongatus* (Figure 2a,b), and in the ENDOR spectra of PS I from *Synechocystis menB*26 substituted with VK_3-h_8 (Figure 2c). However, it is not visible in the ENDOR spectrum of PS I from *Synechocystis menB*26 substituted with VK_3-d_8 (Figure 2d). Therefore, it must arise from one of the α-protons of the second (benzoic) ring and not from protons of the quinone environment or the H-bond proton.

To determine the complete ^{1}H hfc tensors of $A_1^{\bullet-}$, we recorded ENDOR spectra at different magnetic fields to excite molecules with different orientations with respect to the static magnetic field. This was done both for the RP (data not shown) and for photoaccumulated $A_1^{\bullet-}$ (Figure 3); however, a detailed analysis of the orientation-dependent ENDOR spectra was possible only for photoaccumulated $A_1^{\bullet-}$.

The combination of one-dimensional TRIPLE resonance experiments[63] and VMT ENDOR experiments[60] allowed us to determine the signs of the hfc constants that cannot be determined from the ENDOR spectra. The corresponding spectra and their analysis are provided in the Supporting Information (Figures S4−S7). Additional constraints for the simulation of the ENDOR spectra came from the 2D TRIPLE resonance spectra presented below.

Two-Dimensional TRIPLE Spectroscopy. In Figure 4a, a two-dimensional (2D) pulse ^{1}H difference electron−nuclear−nuclear TRIPLE spectrum recorded at the g_y spectral position of photoaccumulated $A_1^{\bullet-}$ in PS I from *T. elongatus* is shown together with a simulation of the most prominent spectral features (Figure 4b). This experiment is a modification of the Davies ENDOR experiment, where an additional RF π-pulse is applied during the mixing time. Whereas the first RF π-pulse is set to a specific frequency, the frequency of the second RF π-pulse is scanned to generate a one-dimensional (1D) TRIPLE spectrum.[63] The difference between this spectrum and the ENDOR spectrum yields the difference TRIPLE spectrum, which exhibits only ENDOR lines that belong to the same electron spin manifold as the one selected by the first RF pulse. The extension in two dimensions is achieved by repeating the experiment for different frequencies of the first RF pulse. The resulting 2D TRIPLE spectrum is mirror-symmetric to its diagonals (assuming that third-order corrections to the Hamiltonian are negligible); thus, only the two lower quadrants are discussed in the following analysis. A detailed introduction to 2D TRIPLE spectroscopy is given in refs 64 and 65. Two-dimensional TRIPLE spectroscopy provides spectral correlations, and offers enhanced resolution due to the spread of the spectrum to a second dimension. In case of $A_1^{\bullet-}$, this is especially helpful at the g_y orientation, where congested powder-type ENDOR signals of various protons are observed. The intense signals on the diagonal (Figure 4a, lower left quadrant) present, in principle, the ENDOR spectrum; the signals on the antidiagonal (lower right quadrant) are due to longitudinal electronic relaxation in the mixing time of the TRIPLE sequence, the so-called indirect TRIPLE effect.[71,86,87] The most prominent ridges located in the two lower quadrants of Figure 4a arise as a result of correlations between methyl group protons and other protons. The orientation of the principal axes of the hfc tensors of the other protons can be determined with higher precision than can be obtained from only the ENDOR spectra, because the orientation of the methyl group proton hfc tensor is well-known. Correlation ridges between protons with the same hfc sign are located in the lower left quadrant (see, e.g., the correlation between the methyl group protons line 1′ and the line 2), whereas correlations between protons with different hfc signs are located in the right quadrant. Of particular interest is the correlation between lines 2′ and 4′. The presence of this correlation ridge clearly shows that these two ENDOR lines are due to different protons. Because line pair 2/2′ is unambiguously assigned to the $A_{||}$ component of the H-bond proton hfc tensor, line pair 4/4′ cannot belong to the H-bond proton, but must arise from one of the α-protons of the quinone with a negative hfc.

Assignment of ENDOR Lines with Weaker Couplings. The simultaneous simulation of 2D TRIPLE and orientation-selected ENDOR spectra allowed us to assign line pair 4/4′ to the α-proton at position 7. This assignment is strongly supported by the DFT results (see below). The unique assignment of hfc constants of the other more weakly coupled protons is more difficult. We have used a comparison with DFT calculations to confirm the predicted assignments.

For the two methylene (CH_2) protons of the phytyl chain, an analysis was not possible. In the RP ENDOR spectra with VK_1 in the A_1 binding site of PS I, no new intense line was detected as compared to the RP ENDOR spectra with VK_3 in the A_1 binding site. We conclude that those methylene protons are not observable in our ENDOR spectra recorded at g_x and g_y position. However, the broad signal with a positive hfc (+1.6 MHz) observed in the 1D TRIPLE spectrum recorded at the g_z spectral position could belong to one of the methylene protons (Figure

S7, spectrum e, Supporting Information). This is in good agreement with the DFT results. The absence of a prominent signal is probably due to the large line width and low intensity of the related resonances. This indicates that the hfc constant shows a distribution, which is probably because of small variations of the dihedral angle of the phytyl chain.[88]

According to the X-ray crystal structure of PS I, only one H-bond to the quinone is present in (neutral) A_1.[4] The orientation-selected ENDOR pattern of this H-bond proton is different from those observed in quinone radical anions in organic solvents.[59,70,89] On the basis of the ENDOR spectra recorded at the g_x spectral position, the hfc of +7.4 MHz (line pair 2/2′, Figures 2 and 3) can be clearly assigned to the $A_{||}$ component of the H-bond proton. This is in excellent agreement with the DFT calculation ($A_{||} = +7.27$ MHz). The $A_{||}$ component of the H-bond proton is hardly observed at the g_z position; thus, the H-bond has to be less than 40° out-of-plane. The $A_\perp$ component is close to $-A_{||}/2$, assuming $a_{iso} \approx 0$ MHz. Line pair 5/5′ (Figures 2 and 3) with a hfc constant of −3.5 MHz is assigned to the $A_\perp$ component of the H-bond proton. This line pair is hardly visible in the ENDOR spectra recorded at $g \geq 2.007$ (Figures 2a,b and 3a) and becomes more pronounced at spectral orientations corresponding to smaller g values (Figure 3b−e). The assignment is less obvious than that of $A_{||}$ component, as several other protons with similar hfc constants have significant contributions to the ENDOR spectra. However, the field dependence of the spectral lines corresponding to the hfc constant of −3.5 MHz can be only attributed to the H-bond proton. Other protons including the α-protons of the benzoic ring or methylene protons of the phytyl chain have distinguishably different field dependences. The fact that the $A_\perp$ component is nearly invisible in the ENDOR spectra recorded at $g \geq 2.007$ indicates that the H-bond is pointing more along the g_x principal axis than along the g_y principal axis. In summary, this orientation dependence shows that the H-bond to the negatively charged quinone is oriented similarly to the X-ray crystal structure.

The line pairs 6/6′ and 8/8′ detected at the g_x orientation (Figures 2 and 3) stem, at least partially, from protons of the protein. This is the only spectral orientation where ENDOR signals from the protein were detected in PS I from *Synechocystis menB*26 substituted with VK_3-d_8. An assignment of these two hfc constants to specific protons on the basis of the data so far presented is not possible. However, assuming only a dipolar coupling of these protein protons to the electron spin, a hfc constant of +2.6 MHz would correspond to a rather small distance (in the range of 3.0−3.5 Å). The protons of the tryptophan residue located at a comparable distance to A_1 might be the origin of these couplings.

DFT Calculations. DFT calculations were performed on a system containing either truncated VK_1 or VK_3 and the backbone atoms of the residues PsaA-L722 and PsaA-A721. Calculations on the B-branch quinone were not conducted because the immediate environments in the two branches are almost identical.[4] In the geometry optimization, the orientation of the truncated phytyl chain and the orientation of the leucine with respect to the quinone were kept fixed, and the H-bond length was optimized (see Supporting Information for details). The geometry optimization of the negatively charged quinone radical anion resulted in a short H-bond length of 1.66 Å, comparable to that found for $Q_A^{\bullet-}$ in photosynthetic reaction centers from *Rhodobacter sphaeroides*.[43,90,91] This is considerably shorter than the H-bond length of 1.74 Å obtained from a restricted geometry optimization using oxidized VK_1 in the A_1 binding site. The shortening of the H-bond upon one-electron reduction of the quinone is similar in magnitude to that observed for $Q_A^{\bullet-}$.[90,91] While the symmetry of the ring is already slightly distorted due to the different substitutions at the carbon atoms 2 and 3, an additional asymmetry is introduced as a result of the single H-bond.

The asymmetric H-bonding by the backbone NH group of the leucine has a significant effect on the calculated spin density distribution and Mulliken spin populations of the molecule compared to the case of symmetric H-bonding to both quinone oxygens, as found, for example, in 2-propanol solution [Figure 5 and Table S2 (Supporting Information)]. It can be seen that unpaired spin density is shifted towards the carbonyl oxygen O_1, which is not involved in the H-bond, whereas the spin population on O_4 is hardly affected. Strong effects are also observed for the carbon atoms C_1, C_2, and C_3: The spin population at the carbon C_2 is increased, whereas the opposite holds for C_1 and C_3. The majority of the unpaired electron is now located at O_1, O_4, C_2, and C_4 and not at O_1, O_4, C_1, and C_4 as found, for example, for the symmetrically hydrogen-bonded $VK_1^{\bullet-}$ in 2-propanol solution. The spin populations in the benzoic ring are found to be small in general. Only atom C_7 shows a significant spin population for $VK_1^{\bullet-}$ in the A_1 site. The spin populations on the neighboring amino acids are well below 1%. In the case of $VK_3^{\bullet-}$, virtually the same effect as for $VK_1^{\bullet-}$ was found (Table S2, Supporting Information).

The calculated proton hfc tensors are given in Table 1 (VK_1) and Table 2 (VK_3). The isotropic hfc constants, which depend on the polarized spin density on the respective nucleus, follow the trend described above. They are larger for the protons covalently bound to carbons C_2, C_5, and C_7 and smaller for those protons bound to carbons C_3, C_6, and C_8. The largest hfc component of the H-bond proton tensor, A_x, is pointing, to a good approximation, along the H-bond. The hfc tensor of the H-bond proton is relatively close to axial symmetry. Despite the rather simple model of the protein binding site, the agreement between the DFT calculations and the experimentally determined ^{1}H hfc tensors was found to be very good. The ^{13}C and ^{17}O hfc constants of $VK_1^{\bullet-}$ and $VK_3^{\bullet-}$ are given in the Supporting Information (Tables S3−S6). The computed **g** tensors are given in Table S1 (also in the Supporting Information). The orientations of the principal axes of the **g** tensor were found to be collinear with the molecular axes system presented in Figure 1c to within ≤3°.

Discussion

Number and Location of Quinones Involved in Electron Transfer. The question of the involvement of both quinones in the electron transfer of PS I has been a controversial matter of discussion in the past (see Introduction). Recently, there seems to be some agreement that, at physiological temperature, both branches are active.[14,17−20] Although the question of directionality is beyond the scope of this study, it is important to determine which quinone is observed under the experimental conditions used here.

It has been shown that the quinone radical anion involved in cyclic electron transfer at low temperature—which is the one observed by time-resolved EPR spectroscopy in the RP $P_{700}^{\bullet+}A_1^{\bullet-}$—is located in the A branch.[14,18,27−29]

Depending on the experimental conditions, the photoaccumulated radical anion $A_1^{\bullet-}$ has been reported to be generated in the A branch, in the B branch, or in both branches.[26−28,39,52−54] In this work, we observed narrow and well-defined ^{1}H ENDOR signals (Figures 2 and 3). Excluding the unlikely event that all ^{1}H hfc tensors are identical for the quinones in both branches,

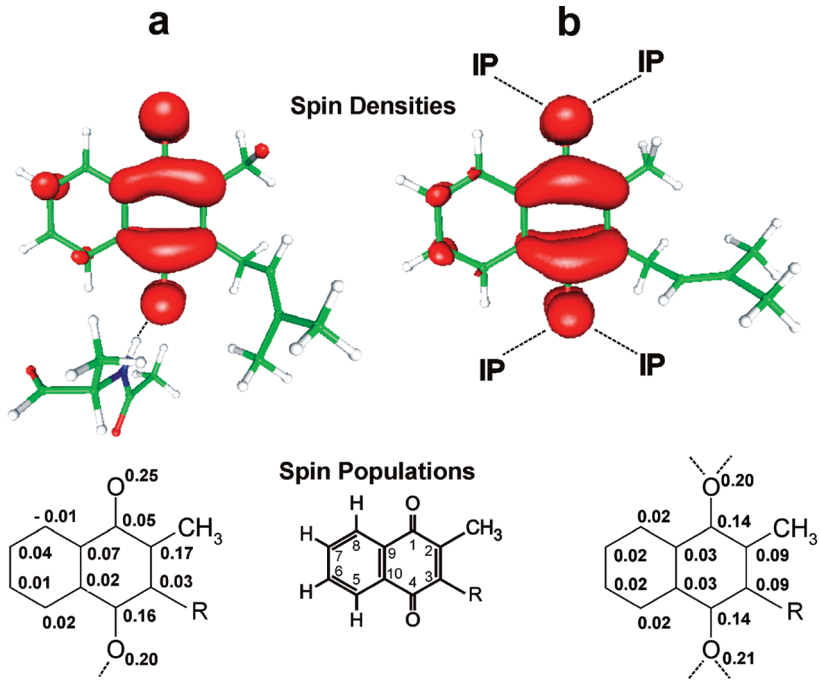

Figure 5. Comparison of calculated electron spin densities (contour level 0.003 e/a_0^3) and Mulliken spin populations of the (ring) carbon and oxygen atoms in $VK_1^{\bullet-}$ (with truncated phytyl chain, labeled R) in different environments (see also Tables S2−S6 in the Supporting Information). Hydrogen bonds are indicated by dashed lines. The electron spin density is the difference between the total density of electrons with α spin minus the total density of electrons with β spin. Hence, the electron spin density depends on all orbitals. The spin density at a nucleus is reflected in the isotropic hyperfine interaction as probed by EPR and ENDOR spectroscopy. Spin populations were obtained from a Mulliken analysis, which attributes fractional amounts of unpaired electrons to each nucleus. The electron spin density distribution and the spin populations in $VK_3^{\bullet-}$ are very similar to the values presented here for $VK_1^{\bullet-}$ (see Supporting Information for details). (a) $VK_1^{\bullet-}$ model in the A_1 binding site, hydrogen-bonded (dashed line) to the leucine residue (PsaA-L722). (b) $VK_1^{\bullet-}$ model in organic solvents, hydrogen-bonded (dashed lines) to four 2-propanol (IP) molecules.[59]

this suggests the observation of a single quinone radical anion. Attempts to directly detect magnetic interactions between two $A_1^{\bullet-}$ radicals in the A and B branches using PELDOR[83,92] and RIDME[93] were not successful. Although this is not conclusive evidence for the absence of a second reduced quinone, it is a further indication that only one quinone radical anion was accumulated under our experimental conditions.

EPR and ^{1}H ENDOR investigations of photoaccumulated $A_1^{\bullet-}$ in two point mutants of *Synechocystis* (PsaA-W697F, PsaB-W677F)[28,94] were carried out in this laboratory. In these mutants, the π-stacked tryptophan was replaced by phenylalanine. Small but notable changes in the ^{1}H ENDOR spectra as compared to that of wild-type PS I were found only for the A-branch mutant and not for the respective B-branch mutant.[95] The number of ^{1}H ENDOR lines of $A_1^{\bullet-}$ remained unchanged in both mutants, indicating that only the A-branch quinone was accumulated.

From these results, we conclude that, under the experimental conditions used in this study, only the A-branch quinone is detected by EPR spectroscopy. This holds both for the RP $P_{700}^{\bullet+}A_1^{\bullet-}$ and for photoaccumulated $A_1^{\bullet-}$.

Electronic Structures of $VK_1^{\bullet-}$/$VK_3^{\bullet-}$ in Organic Solvents and in the $A_1^{\bullet-}$ Binding Site: Influence of the Protein Surrounding. In a previous study, we investigated several different quinone radical anions in the hydrogen-bonding solvent 2-propanol.[59] In that study, DFT calculations proved to be quite accurate in predicting the hfc tensors of the quinone protons. The calculation of hfc tensors for the solvent protons involved in in-plane hydrogen bonding provided values very close to those determined experimentally. An alternating effect of the spin density distribution within the quinone upon asymmetric H-bonding (two H-bonds to O_4, one to O_1) was observed. An increase in the spin density at positions 2, 5, and 7 and a decrease at positions 3, 6, and 8 were found, as compared to the values for the symmetrically hydrogen-bonded species. As shown for $VK_1^{\bullet-}$ in frozen 2-propanol, out-of-plane H-bonds had a similar effect on the spin density distribution as the in-plane H-bonds.

For the quinone radical anion in the A_1 site, DFT calculations showed that a single-sided H-bond is required to obtain good agreement with the experimental data (Tables 1 and 2). This finding is also supported by previous DFT calculations[96,97] and the results obtained for $Q_A^{\bullet-}$ in the bacterial photosynthetic reaction centers,[41,43,90,91] which showed that asymmetric H-bonding can induce the unusual asymmetric spin density distribution observed in $A_1^{\bullet-}$. Especially the ^{1}H hfc constants are an excellent probe for the asymmetry of the spin density distribution in the quinone. The presence of only one H-bond is also strongly supported by the high-resolution crystal structure of PS I with neutral A_1.[4]

In previous studies,[39,96,98] the possibility was discussed that an apolar and aprotic environment opposed to a protic and polar environment could explain the extremely low redox potential of A_1 and the large g_x value. In these studies, the apolar environment of the quinone in the A_1 binding site was modeled using a mixture of the apolar and aprotic solvents dimethoxyethane (DME) and 2-methyltetrahydrofuran (MTHF). This shifted the redox potential of VK_1 and the **g** tensor to values very close to what was found for A_1. However, no asymmetry in the spin density distribution was induced by this environment. Thus, the low polarizability cannot account for the spin density distribution in $A_1^{\bullet-}$. Consequently, the asymmetric H-bond is the key factor for understanding the spin density distribution in $A_1^{\bullet-}$.

DFT calculations with VK_3 instead of VK_1 in the identical binding site also showed good agreement with the experimentally determined hfc constants (Table 2). The two quinones experience similar shifts of the spin density in the A_1 binding site as compared to the symmetric hydrogen-bonded situation found in frozen 2-propanol solution. From this result, we can conclude that VK_1 and VK_3 are bound in very similar ways by the protein.

The Proton in the Hydrogen Bond. All principal components of the hfc tensor of the proton in the H-bond have been determined in this work; the isotropic hfc constant is small, and the H-bond is not severely out-of-plane (Tables 1 and 2). Hence, the length of the H-bond can be estimated using the point-dipole approximation[99,100] according to the expression

$$A_{\mathrm{dip}} = \frac{g_e \beta_e g_N \beta_N}{hr^3} \rho_S (3 \cos^2 \delta - 1) \qquad (1)$$

where g_e and g_N are the electron and nuclear g values, respectively; β_e and β_N are the electron and nuclear magnetons, respectively; ρ_S is the spin population at the quinone oxygen; δ is the angle between the applied magnetic field and the direction of the H-bond; and r is the length of the H-bond in angstroms. It was found previously that the agreement between calculated and experimentally determined spin populations on the oxygens of quinone radical anions is very good.[59] The spin population on the oxygen at position 4 was taken from the DFT calculations ($\rho_{O4} = 0.20$), as no experimental value is available. Estimations of the spin density from ^{17}O-labeled VK_3 yielded similar values.[101] Using eq 1 and the experimentally determined hfc constants of the H-bond proton (Table 1), a distance of 1.64 Å was calculated. This value is in good agreement with the distance of 1.66 Å obtained by the restricted geometry optimization, where the distance between O_4 and the amide nitrogen of leucine was kept constant. Thus, in the reduced quinone in the A_1 binding site, the H-bond is shorter than in neutral quinone occupying the same site (1.74 Å). The length of this H-bond is similar to those of the two H-bonds found for $Q_A^{\bullet-}$ in bacterial photosynthetic RCs.[43,90,91]

A determination of the H-bond proton hfc tensor has been attempted several times in the past, and different and controversial assignments have been obtained. Teutloff performed a pulse X-band ^1H ENDOR study of the photoaccumulated radical anion $A_1^{\bullet-}$ and the RP in PS I from *T. elongatus* and assigned one axial tensor with an $A_{||}$ component of (+)14.8 MHz and an $A_\perp$ component of (−)4.9 MHz to the H-bond proton ($a_{\mathrm{iso}} = +1.7$ MHz).[96] Such a hfc tensor would be an indication of an unusually short and strong H-bond. It is important to note that the 14.8 MHz component was not detected in the RP ENDOR spectra. In a later work by the same authors, the large component of the hfc tensor was assigned only tentatively to the H-bond proton. This was explained by the possibility that this hfc constant could arise from a contribution of the chlorophyll radical $A_0^{\bullet-}$ in the photoaccumulated samples.[39]

Heathcote and co-workers investigated the photoaccumulated radical anion $A_1^{\bullet-}$ using CW X-band ENDOR and special TRIPLE spectroscopy.[37,52–54] Their analyses were based on the assumption that the two quinones in the A or B branch could be photoaccumulated selectively. They proposed two H-bonds per $A_1^{\bullet-}$ radical anion, with different hfc constants depending on the species from which the PS I complexes where isolated.[37,52–54,102] A hfc constant of about (+)12 MHz was assigned to the large component of the H-bond proton hfc tensor, close to the hfc constant reported by Teutloff in ref 96. Under the experimental conditions used in this study, only the A-branch quinone is observed by EPR spectroscopy, both in the RP and in photoaccumulated PS I samples. Considering the data presented in our work, it seems to us that the ENDOR data previously reported by Heathcote and co-workers[37,52−54] were overinterpreted, owing to the low spectral resolution of powder-type ^1H ENDOR spectra at X-band, and possible contamination with other radicals, such as $A_0^{\bullet-}$. Therefore, in the following, only the case of a single H-bond to the quinone radical anion is discussed.

In a previous study, the photoaccumulated radical anion of fully deuterated VK_3 in the A_1 binding site of PS I from the *menB* mutant of *Synechocystis* in protonated buffer was investigated by ENDOR spectroscopy at Q-band.[49] The authors assigned hfc constants of $A_{||} = (+)7.7$ MHz and $A_\perp = (-)4.9$ MHz to the proton of the H-bond. Note, that no measurements of $A_1^{\bullet-}$ in the RP were performed.

A problem encountered in previous studies was the presence of the chlorophyll radical anion $A_0^{\bullet-}$ in photoaccumulated PS I samples.[26,28,49,54] Since protons of $A_0^{\bullet-}$ have intense ENDOR signals,[82,103,104] even a small contribution of $A_0^{\bullet-}$ obscures the broad and weak ENDOR lines of the proton in the H-bond to $A_1^{\bullet-}$ (see Supporting Information). This is especially problematic for X-band studies, where the EPR spectra of $A_1^{\bullet-}$ and $A_0^{\bullet-}$ overlap, making it impossible to selectively excite either radical. This is significantly improved at Q-band, owing to the larger g anisotropy of $A_1^{\bullet-}$ compared to $A_0^{\bullet-}$. ENDOR spectra of pure $A_1^{\bullet-}$ can be obtained at spectral positions around g_x. This holds, of course, only for $A_1^{\bullet-}$ samples containing a small contamination of $A_0^{\bullet-}$.

The large ^1H hfc constants of $A_0^{\bullet-}$ [82,103,104] are within the range of the large hfc constants that were observed by Teutloff[96] and Heathcote et al.,[37,50,52] which were assigned to the H-bond proton. It was clearly shown here on photoaccumulated $A_1^{\bullet-}$ samples with a negligible contamination of $A_0^{\bullet-}$ that no signals from hfc constants larger than that of the methyl group were present at spectral positions between g_x and g_y. In the RP EPR and ENDOR spectra, where a contamination with $A_0^{\bullet-}$ is not present, these large hfc constants were not observed. From this, we conclude that these hfc constants arise not from the proton H-bonded to $A_1^{\bullet-}$ but from $A_0^{\bullet-}$ protons. Thus, previous assignments[37,50,52−54,96,102] need to be revised.

For the $A_\perp$ component of the H-bond proton tensor, a variety of hfc constants have been proposed. In some studies, the (−)4.9 MHz hfc constant was attributed to the H-bond proton.[37,39,49,96] In our study, based on ENDOR data and DFT calculations, the line pair 4/4′ in Figures 2 and 3 (~ -4.9 MHz hfc constant) is assigned to the α-proton at position 7 in the benzoic ring. In particular, the absence of this intense line pair in the RP ENDOR spectra of PS I from *Synechocystis menB*26 mutant substituted with VK_3-d_8 indicates that this line pair does not arise from the H-bond proton. Furthermore, this assignment is also supported by the 2D TRIPLE simulations (Figure 4). Teutloff et al.[39] explicitly mentioned in their work that they assigned this line pair to the H-bond proton, because they did not expect that one of the α-protons from the second ring could have such a large hfc constant. Such an explanation cannot account for the results of Pushkar et al.,[49] given that they used a fully deuterated quinone (VK_3-d_8) in the A_1 binding site of *Synechocystis menB*26 mutant PS I. However, their photoaccumulated PS I samples had a strong $A_0^{\bullet-}$ contamination. The lines due to protons with large hfc constants indicative of $A_0^{\bullet-}$ [82,103,104] are clearly visible in the ENDOR spectra. Indeed, the contamination

with $A_0^{\bullet-}$ is so strong that even at the g_x spectral position the contribution of $A_0^{\bullet-}$ to the ENDOR spectrum is not negligible. The ^{1}H ENDOR spectrum of $A_0^{\bullet-}$ has intense signals arising from a hfc constant of about 4.9 MHz,[82,103,104] which is discussed in the Supporting Information. Thus, the assignment of the 4.9 MHz (line pair 4/4′) hfc constant to the $A_\perp$ component of the H-bond proton hfc tensor[49] cannot be correct.

Hence, we can assign with confidence the ^{1}H hfc tensor with $A_{||} = +7.4$ MHz and $A_\perp = -3.5$ MHz to the proton in the single hydrogen bond to the radical anions of VK_1 and VK_3 in PS I. This assignment solves a long-standing problem in this field.

Summary and Conclusions

A comprehensive Q-band EPR, ENDOR, and TRIPLE investigation of $A_1^{\bullet-}$, both in photoaccumulated samples and in the spin-polarized radical pair $P_{700}^{\bullet+}A_1^{\bullet-}$ of cyanobacterial PS I from *T. elongatus*, is reported here. In addition, PS I from the *Synechocystis menB* mutant substituted with fully protonated and fully deuterated VK_3 in the A_1 binding site was studied to aid in the assignment of ^{1}H ENDOR lines. DFT calculations were performed, using a model of the A_1 binding site consisting of a VK_1 or VK_3 molecule hydrogen-bonded to a leucine residue. They are in good agreement with the experimental data showing that the presence of only one strong H-bond can fully account for the asymmetry of the spin density distribution in the radical anion $A_1^{\bullet-}$.

It was further shown that, under the experimental condition used in this work, the A-branch quinone is observed both in photoaccumulated $A_1^{\bullet-}$ and in the RP $P_{700}^{\bullet+}A_1^{\bullet-}$. For the first time, ENDOR lines belonging to the α-protons of the second (benzoic) ring were assigned along with the methyl group protons. The proton hfc constants determined for the photoaccumulated radical anion and for the radical pair turned out to be nearly identical, indicating similar binding situations for the two species.

The hfc tensor of the H-bond proton was determined by resolving the $A_0^{\bullet-}$ contamination problem of previous studies and correcting previously published assignments. A comparative analysis of $A_1^{\bullet-}$ and $P_{700}^{\bullet+}A_1^{\bullet-}$ ENDOR spectra of PS I from *T. elongatus* and from the *Synechocystis menB* mutant with fully deuterated and fully protonated VK_3, in combination with the DFT results, confirmed the presence of only one strong H-bond to the quinone. The length of the H-bond was calculated using the point-dipole approximation to be 1.64 Å, close to the result of the DFT calculations, which gave 1.66 Å. This corresponds to a relatively short and strong hydrogen bond.

Abbreviations

A_1, quinone electron acceptor in PS I; Chl *a*, chlorophyll *a*; ENDOR, electron−nuclear double resonance; EPR, electron paramagnetic resonance; hfc, hyperfine coupling; P_{700}, Chl *a*/Chl *a*′ heterodimer in PS I; PELDOR, pulsed electron−electron double resonance; PQ_9, plastoquinone-9; PS I, photosystem I; RIDME, relaxation-induced dipolar modulation enhancement; RP, radical pair; TRIPLE, electron−nuclear−nuclear triple resonance; VK_1, vitamin K_1 or 2-methyl-3-phytyl-1,4-naphthoquinone or phylloquinone; VK_3, vitamin K_3 or 2-methyl-1,4-naphthoquinone; VK_3-d_8, fully deuterated vitamin K_3; VK_3-h_8, fully protonated vi tamin K_3.

Acknowledgment. This work is dedicated to our long-time colleague Professor Achim Trebst (Ruhr-Universität Bochum, Bochum, Germany) on the occasion of his 80th birthday. We thank J. Kern, J. Frank (TU Berlin, Berlin, Germany) and P. Fromme (TU Berlin, now Arizona State University, Tempe, AZ) for providing trimeric PS I from *T. elongatus*. The clone of *Synechocystis menB*26 was a kind gift of J. H. Golbeck and W. Johnson (The Pennsylvania State University, University Park, PA). Deuterated vitamin K_3 is a courtesy of H. Zimmermann (MPI Heidelberg, Heidelberg, Germany). G. Klihm (MPI Mülheim, Mülheim an der Ruhr, Germany) is acknowledged for technical assistance. This work was supported by the DFG (SFB 663, TP A7; SFB 498, TP A3) and the Max Planck Society.

Supporting Information Available: Chemical structures of the truncated vitamin K_1 used in the DFT calculations, vitamin K_3, and plastoquinone-9 with numbering schemes; comprehensive description of Materials and Methods; additional EPR, ENDOR, and TRIPLE spectra; spin densities and spin populations of vitamin K_1 and vitamin K_3 in the A_1 binding site of PS I and in organic solvents; and ^{13}C and ^{17}O hfc constants. This material is available free of charge via the Internet at http://pubs.acs.org.

References and Notes

(1) Blankenship, R. E. *Molecular Mechanisms of Photosynthesis*, 1st ed.; Blackwell Science Limited: Oxford, 2002.

(2) Archer, M. D., Barber, J., Eds. *Molecular to Global Photosynthesis*; Series on Photoconversion of Solar Energy; Imperial College Press: London, 2004; Vol. 2.

(3) Golbeck, J. H., Ed.; *Photosystem I: The Light-Driven Plastocyanin: Ferredoxin Oxidoreductase*; Advances in Photosynthesis and Respiration Series; Springer: Dordrecht, The Netherlands, 2006; Vol. 24.

(4) Jordan, P.; Fromme, P.; Witt, H. T.; Klukas, O.; Saenger, W.; Krauss, N. *Nature* **2001**, *411*, 909–917.

(5) Amunts, A.; Drory, O.; Nelson, N. *Nature* **2007**, *447*, 58–63.

(6) Savikhin, S. Ultrafast Optical Spectroscopy of Photosystem I. In Golbeck, J. H., Ed.; *Photosystem I: The Light-Driven Plastocyanin: Ferredoxin Oxidoreductase*; Advances in Photosynthesis and Respiration Series; Springer: Dordrecht, The Netherlands, 2006; Vol. 24, pp 155−175.

(7) Holzwarth, A. R.; Müller, M. G.; Niklas, J.; Lubitz, W. *Biophys. J.* **2006**, *90*, 552–565.

(8) Holzwarth, A. R.; Müller, M. G.; Niklas, J.; Lubitz, W. *J. Phys. Chem. B* **2005**, *109*, 5903–5911.

(9) Müller, M.; Niklas, J.; Lubitz, W.; Holzwarth, A. R. *Biophys. J.* **2003**, *85*, 3899–3822.

(10) Brettel, K.; Leibl, W. *Biochim. Biophys. Acta* **2001**, *1507*, 100–114.

(11) Antonkine, M. L.; Golbeck, J. H. Molecular Interactions of the Stromal Subunit PsaC with the PsaA/PsaB Heterodimer. In *Photosystem I: The Light-Driven Plastocyanin: Ferredoxin Oxidoreductase*; Advances in Photosynthesis and Respiration Series; Springer: Dordrecht, The Netherlands, 2006; Vol. 24, pp 79−98.

(12) Vassiliev, I. R.; Antonkine, M. L.; Golbeck, J. H. *Biochim. Biophys. Acta* **2001**, *1507*, 139–160.

(13) Brettel, K. *Biochim. Biophys. Acta* **1997**, *1318*, 322–373.

(14) Stehlik, D. Transient EPR Spectroscopy as Applied to Light-Induced Functional Intermediates along the Electron Transfer Pathway in Photosystem I. In *Photosystem I: The Light-Driven Plastocyanin: Ferredoxin Oxidoreductase*; Advances in Photosynthesis and Respiration Series; Springer: Dordrecht, The Netherlands, 2006; Vol. 24, pp 361−386.

(15) van der Est, A. *Biochim. Biophys. Acta* **2001**, *1507*, 212–225.

(16) Stehlik, D.; Möbius, K. *Annu. Rev. Phys. Chem.* **1997**, *48*, 745–784.

(17) Holzwarth A. R.; Müller, M. G.; Slavov, C.; Luthra, R.; Redding, K. Ultrafast Energy and Electron Transfer in Photosystem I−Direct Evidence for Two-Branched Electron Transfer. In *Ultrafast Phenomena XV*; Corkum, P., Jonas, D., Miller, R. J. D., Weiner, A. M., Eds.; Springer Series in Chemical Physics; Springer: Berlin, 2007; Vol. 88, pp 471−473.

(18) Redding, K.; van der Est, A. The Directionality of Electron Transport in Photosystem I. In *Photosystem I: The Light-Driven Plastocyanin: Ferredoxin Oxidoreductase*; Advances in Photosynthesis and Respiration Series; Springer: Dordrecht, The Netherlands, 2006; Vol. 24, pp 413−437.

(19) van der Est, A. Electron Transfer Involving Phylloquinone in Photosystem I. In *Photosystem I: The Light-Driven Plastocyanin: Ferredoxin Oxidoreductase*; Advances in Photosynthesis and Respiration Series; Springer: Dordrecht, The Netherlands, 2006; Vol. 24, pp 387−411.

(20) Li, Y.; van der Est, A.; Lucas, M. G.; Ramesh, V. M.; Gu, F.; Petrenko, A.; Lin, S.; Webber, A. N.; Rappaport, F.; Redding, K. *Proc. Natl. Acad. Sci. U.S.A.* **2006**, *103*, 2144–2149.

(21) Santabarbara, S.; Kuprov, I.; Fairclough, W. V.; Purton, S.; Hore, P. J.; Heathcote, P.; Evans, M. C. W. *Biochemistry* **2005**, *44*, 2119–2128.

(22) Bautista, J. A.; Rappaport, F.; Guergova-Kuras, M.; Cohen, R. O.; Golbeck, J. H.; Wang, J. Y.; Beal, D.; Diner, B. A. *J. Biol. Chem.* **2005**, *280*, 20030–20041.

(23) Poluektov, O. G.; Utschig, L. M.; Dubinskij, A. A.; Thurnauer, M. C. *J. Am. Chem. Soc.* **2005**, *127*, 4049–4059.

(24) Guergova-Kuras, M.; Boudreaux, B.; Joliot, A.; Joliot, P.; Redding, K. *Proc. Natl. Acad. Sci. U.S.A.* **2001**, *98*, 4437–4442.

(25) Joliot, P.; Joliot, A. *Biochemistry* **1999**, *38*, 11130–11136.

(26) Yang, F.; Shen, G. Z.; Schluchter, W. M.; Zybailov, B. L.; Ganago, A. O.; Vassiliev, I. R.; Bryant, D. A.; Golbeck, J. H. *J. Phys. Chem. B* **1998**, *102*, 8288–8299.

(27) Boudreaux, B.; MacMillan, F.; Teutloff, C.; Agalarov, R.; Gu, F. F.; Grimaldi, S.; Bittl, R.; Brettel, K.; Redding, K. *J. Biol. Chem.* **2001**, *276*, 37299–37306.

(28) Xu, W.; Chitnis, P.; Valieva, A.; van der Est, A.; Pushkar, Y. N.; Krzystyniak, M.; Teutloff, C.; Zech, S. G.; Bittl, R.; Stehlik, D.; Zybailov, B.; Shen, G. Z.; Golbeck, J. H. *J. Biol. Chem.* **2003**, *278*, 27864–27875.

(29) Zech, S.; Hofbauer, W.; Kamlowski, A.; Fromme, P.; Stehlik, D.; Lubitz, W.; Bittl, R. *J. Phys. Chem. B* **2000**, *104*, 9728–9739.

(30) Vos, M. H.; Vangorkom, H. J. *Biophys. J.* **1990**, *58*, 1547–1555.

(31) Setif, P.; Bottin, H. *Biochemistry* **1989**, *28*, 2689–2697.

(32) Pushkar, Y. N.; Karyagina, I.; Stehlik, D.; Brown, S.; van der Est, A. *J. Biol. Chem.* **2005**, *280*, 12382–12390.

(33) van der Est, A.; Pushkar, Y. N.; Karyagina, I.; Fonovic, B.; Dudding, T.; Niklas, J.; Lubitz, W.; Golbeck, J. H. *Appl. Magn. Reson.,* in press.

(34) Semenov, A. Y.; Vassiliev, I. R.; van der Est, A.; Mamedov, M. D.; Zybailov, B.; Shen, G. Z.; Stehlik, D.; Diner, B. A.; Chitnis, P. R.; Golbeck, J. H. *J. Biol. Chem.* **2000**, *275*, 23429–23438.

(35) Sakuragi, Y.; Zybailov, B.; Shen, G.; Jones, A. D.; Chitnis, P. R.; van der Est, A.; Bittl, R.; Zech, S.; Stehlik, D.; Golbeck, J. H.; Bryant, J. A. *Biochemistry* **2002**, *41*, 394–405.

(36) Zybailov, B.; van der Est, A.; Zech, S. G.; Teutloff, C.; Johnson, T. W.; Shen, G. Z.; Bittl, R.; Stehlik, D.; Chitnis, P. R.; Golbeck, J. H. *J. Biol. Chem.* **2000**, *275*, 8531–8539.

(37) Rigby, S. E. J.; Evans, M. C. W.; Heathcote, P. *Biochemistry* **1996**, *35*, 6651–6656.

(38) van der Est, A.; Prisner, T.; Bittl, R.; Fromme, P.; Lubitz, W.; Möbius, K.; Stehlik, D. *J. Phys. Chem. B* **1997**, *101*, 1437–1443.

(39) Teutloff, C.; Bittl, R.; Lubitz, W. *Appl. Magn. Reson.* **2004**, *26*, 5–21.

(40) Santabarbara, S.; Heathcote, P.; Evans, M. C. W. *Biochim. Biophys. Acta* **2005**, *1708*, 283–310.

(41) Lubitz, W.; Feher, G. *Appl. Magn. Reson.* **1999**, *17*, 1–48.

(42) Lubitz, W.; Abresch, E. C.; Debus, R. J.; Isaacson, R. A.; Okamura, M. Y.; Feher, G. *Biochim. Biophys. Acta* **1985**, *808*, 464–469.

(43) Flores, M.; Isaacson, R.; Abresch, E.; Calvo, R.; Lubitz, W.; Feher, G. *Biophys. J.* **2007**, *92*, 671–682.

(44) Flores, M.; Isaacson, R.; Abresch, E.; Calvo, R.; Lubitz, W.; Feher, G. *Biophys. J.* **2006**, *90*, 3356–3362.

(45) Goldfarb, D.; Arieli, D. *Annu. Rev. Biophys. Biomol. Struct.* **2004**, *33*, 441–468.

(46) Lubitz, W.; Lendzian, F.; Bittl, R. *Acc. Chem. Res.* **2002**, *35*, 313–320.

(47) Witt, H.; Schlodder, E.; Teutloff, C.; Niklas, J.; Bordignon, E.; Carbonera, D.; Kohler, S.; Labahn, A.; Lubitz, W. *Biochemistry* **2002**, *41*, 8557–8569.

(48) Kurreck, H.; Kirste, B.; Lubitz, W. *Electron Nuclear Double Resonance Spectroscopy of Radicals in Solution: Applications to Organic and Biological Chemistry*; Methods in Stereochemical Analysis Series; Marchand, A. P., Ed.; VCH Publishers: Weinheim, Germany, 1988.

(49) Pushkar, Y. N.; Stehlik, D.; van Gastel, M.; Lubitz, W. *J. Mol. Struct.* **2004**, *700*, 233–241.

(50) Rigby, S. E. J.; Evans, M. C. W.; Heathcote, P. *Biochim. Biophys. Acta* **2001**, *1507*, 247–259.

(51) Fursman, C. E.; Teutloff, C.; Bittl, R. *J. Phys. Chem. B* **2002**, *106*, 9679–9686.

(52) Rigby, S. E. J.; Muhiuddin, I. P.; Evans, M. C. W.; Purton, S.; Heathcote, P. *Biochim. Biophys. Acta* **2002**, *1556*, 13–20.

(53) Purton, S.; Stevens, D. R.; Muhiuddin, I. P.; Evans, M. C. W.; Carter, S.; Rigby, S. E. J.; Heathcote, P. *Biochemistry* **2001**, *40*, 2167–2175.

(54) Fairclough, W. V.; Forsyth, A.; Evans, M. C. W.; Rigby, S. E. J.; Purton, S.; Heathcote, P. *Biochim. Biophys. Acta* **2003**, *1606*, 43–55.

(55) Johnson, T. W.; Zybailov, B.; Jones, A. D.; Bittl, R.; Zech, S.; Stehlik, D.; Golbeck, J. H.; Chitnis, P. R. *J. Biol. Chem.* **2001**, *276*, 39512–39521.

(56) Johnson, T. W.; Shen, G.; Zybailov, B.; Kolling, D.; Reategui, R.; Beauparlant, S.; Vassiliev, I. R.; Bryant, D. A.; Jones, A. D.; Golbeck, J. H.; Chitnis, P. R. *J. Biol. Chem.* **2000**, *275*, 8523–8530.

(57) Sakuragi, Y.; Bryant, D. A. Genetic Manipulation of Quinone Biosynthesis in Cyanobacteria. In *Photosystem I: The Light-Driven Plastocyanin: Ferredoxin Oxidoreductase*; Advances in Photosynthesis and Respiration Series; Springer: Dordrecht, The Netherlands, 2006; Vol. 24, pp 205−222.

(58) Pushkar, Y. N.; Golbeck, J. H.; Stehlik, D.; Zimmermann, H. *J. Phys. Chem. B* **2004**, *108*, 9439–9448.

(59) Epel, B.; Niklas, J.; Sinnecker, S.; Zimmermann, H.; Lubitz, W. *J. Phys. Chem. B* **2006**, *110*, 11549–11560.

(60) Epel, B.; Niklas, J.; Antonkine, M. L.; Lubitz, W. *Appl. Magn. Reson.* **2006**, *30*, 311–327.

(61) Epel, B.; Poppl, A.; Manikandan, P.; Vega, S.; Goldfarb, D. *J. Magn. Reson.* **2001**, *148*, 388–397.

(62) Epel, B.; Manikandan, P.; Kroneck, P. M. H.; Goldfarb, D. *Appl. Magn. Reson.* **2001**, *21*, 287–297.

(63) Mehring, M.; Höfer, P.; Grupp, A. *Ber. Bunsen-Ges. Phys. Chem.* **1987**, *91*, 1132–1137.

(64) Goldfarb, D.; Epel, B.; Zimmermann, H.; Jeschke, G. *J. Magn. Reson.* **2004**, *168*, 75–87.

(65) Epel, B.; Goldfarb, D. *J. Magn. Reson.* **2000**, *146*, 196–203.

(66) Fromme, P.; Witt, H. T. *Biochim. Biophys. Acta* **1998**, *1365*, 175–184.

(67) Shen, G. Z.; Zhao, J. D.; Reimer, S. K.; Antonkine, M. L.; Cai, Q.; Weiland, S. M.; Golbeck, J. H.; Bryant, D. A. *J. Biol. Chem.* **2002**, *277*, 20343–20354.

(68) MacMillan, F.; Hanley, J.; van der Weerd, L.; Knüpling, M.; Un, S.; Rutherford, A. W. *Biochemistry* **1997**, *36*, 9297–9303.

(69) Shen, G. Z.; Antonkine, M. L.; van der Est, A.; Vassiliev, I. R.; Brettel, K.; Bittl, R.; Zech, S. G.; Zhao, J. D.; Stehlik, D.; Bryant, D. A.; Golbeck, J. H. *J. Biol. Chem.* **2002**, *277*, 20355–20366.

(70) Sinnecker, S.; Reijerse, E.; Neese, F.; Lubitz, W. *J. Am. Chem. Soc.* **2004**, *126*, 3280–3290.

(71) Silakov, A.; Reijerse, E. J.; Albracht, S. P. J.; Hatchikian, E. C.; Lubitz, W. *J. Am. Chem. Soc.* **2007**, *129*, 11447–11458.

(72) Sienkiewicz, A.; Smith, B. G.; Veselov, A.; Scholes, C. P. *Rev. Sci. Instrum.* **1996**, *67*, 2134–2138.

(73) Davies, E. R. *Phys. Lett.* **1974**, *47A*, 1–2.

(74) *MATLAB*, R13; The MathWorks, Inc.: Natick, MA, 2002.

(75) Stoll, S.; Schweiger, A. *J. Magn. Reson.* **2005**, *177*, 390–403.

(76) Kandrashkin, Y. E.; Salikhov, K. M.; van der Est, A.; Stehlik, D. *Appl. Magn. Reson.* **1998**, *15*, 417–447.

(77) Salikhov, K. M.; Schlüpmann, J.; Plato, M.; Möbius, K. *Chem. Phys.* **1997**, *215*, 23–35.

(78) Kandrashkin, Y. E.; Salikhov, K. M.; Stehlik, D. *Appl. Magn. Reson.* **1997**, *12*, 141–166.

(79) Stehlik, D.; Bock, C. H.; Petersen, J. *J. Phys. Chem.* **1989**, *93*, 1612–1619.

(80) Angerhofer, A.; Bittl, R. *Photochem. Photobiol.* **1996**, *63*, 11–38.

(81) Hore, P. J. Analysis of Polarized Electron Paramagnetic Resonance Spectra. In *Advanced EPR−Applications in Biology and Biochemistry*; Hoff, A. J., Ed.; Elsevier: Amsterdam, 1989; Chapter 12, pp 405−440.

(82) Rigby, S. E. J.; Muhiuddin, I. P.; Santabarbara, S.; Evans, M. C. W.; Heathcote, P. *Chem. Phys.* **2003**, *294*, 319–328.

(83) Schweiger, A.; Jeschke, G. *Principles of Pulse Electron Paramagnetic Resonance*; Oxford University Press: New York, 2001.

(84) Hoffman, B. M.; Martinsen, J.; Venters, R. A. *J. Magn. Reson.* **1984**, *59*, 110–123.

(85) Rist, G.; Hyde, J. S. *J. Chem. Phys.* **1970**, *52*, 4633–4643.

(86) Höfer, P. Entwicklung von Puls-ENDOR-Verfahren und ihre Anwendung auf Polyazetylen. Doctoral Thesis, Universität Stuttgart, Stuttgart, Germany, 1988.

(87) Silakov, A. Investigation of the active site of the [FeFe] hydrogenase from *Desulfovibrio desulfuricans*. Doctoral Thesis, Heinrich-Heine-Universität Düsseldorf, Düsseldorf, Germany, 2007.

(88) Himo, F.; Babcock, G. T.; Eriksson, L. A. *J. Phys. Chem. A* **1999**, *103*, 3745–3749.

(89) Flores, M.; Isaacson, R.; Calvo, R.; Feher, G.; Lubitz, W. *Chem. Phys.* **2003**, *294*, 401–413.

(90) Sinnecker, S.; Flores, M.; Lubitz, W. *Phys. Chem. Chem. Phys.* **2006**, *8*, 5659–5670.

(91) Fritscher, J.; Prisner, T. F.; MacMillan, F. *Appl. Magn. Reson.* **2006**, *30*, 251–268.

(92) Jeschke, G. *ChemPhysChem* **2002**, *3*, 927–932.

(93) Kulik, L. V.; Dzuba, S. A.; Grigoryev, I. A.; Tsvetkov, Y. D. *Chem. Phys. Lett.* **2001**, *343*, 315–324.

(94) Xu, W.; Chitnis, P. R.; Valieva, A.; van der Est, A.; Brettel, K.; Guergova-Kuras, M.; Pushkar, Y. N.; Zech, S. G.; Stehlik, D.; Shen, G. Z.; Zybailov, B.; Golbeck, J. H. *J. Biol. Chem.* **2003**, *278*, 27876–27887.

(95) Niklas, J.; Antonkine, M. L.; Shen, G.; Epel, B., manuscript in preparation.

(96) Teutloff, C. Untersuchungen zur Bindung des sekundären Akzeptors in Photosystem I mit Methoden der EPR-Spektroskopie. Doctoral Thesis, Technische Universität Berlin, Berlin, Germany, 2004.

(97) O'Malley, P. J. *Biochim. Biophys. Acta* **1999**, *1411*, 101–113.

(98) Teutloff, C.; Hofbauer, W.; Zech, S. G.; Stein, M.; Bittl, R.; Lubitz, W. *Appl. Magn. Reson.* **2001**, *21*, 363–379.

(99) Atherton, N. M. *Principles of Electron Spin Resonance*; Ellis Horwood & PTR Prentice Hall: New York, 1993.

(100) Weil, J. A.; Bolton, J. R. *Electron Paramagnetic Resonance: Elementary Theory and Practical Applications*, 2nd ed.; John Wiley & Sons, Inc.: New York, 2007.

(101) Pushkar, Y. N.; Ayzatulin, O.; Stehlik, D. *Appl. Magn. Reson.* **2005**, *28*, 195–211.

(102) Evans, M. C. W.; Purton, S.; Patel, V.; Wright, D.; Heathcote, P.; Rigby, S. E. J. *Photosynth. Res.* **1999**, *61*, 33–42.

(103) Forman, A.; Davis, M. S.; Fujita, I.; Hanson, L. K.; Smith, K. M.; Fajer, J. *Isr. J. Chem.* **1981**, *21*, 265–269.

(104) Fajer, J.; Davis, M. S.; Forman, A.; Klimov, V. V.; Dolan, E.; Ke, B. *J. Am. Chem. Soc.* **1980**, *102*, 7143–7145.

(105) Muhiuddin, I. P.; Rigby, S. E. J.; Evans, M. C. W.; Amesz, J.; Heathcote, P. *Biochemistry* **1999**, *38*, 7159–7167.

(106) Burghaus, O.; Plato, M.; Rohrer, M.; Möbius, K.; MacMillan, F.; Lubitz, W. *J. Phys. Chem.* **1993**, *97*, 7639–7647.

(107) Isaacson, R. A.; Lendzian, F.; Abresch, E. C.; Lubitz, W.; Feher, G. *Biophys. J.* **1995**, *69*, 311–322.

JP901890Z